Mechanism for Amplitude Alternans in Electrocardiograms and the Initiation of Spatiotemporal Chaos

Diandian Diana Chen, Richard A. Gray, Ilija Uzelac, Conner Herndon, and Flavio H. Fenton

Phys. Rev. Lett. **118**, 168101 — Published 20 April 2017

DOI: 10.1103/PhysRevLett.118.168101

A Mechanism for QRS Amplitude Alternans in Electrocardiograms and the Initiation of Spatiotemporal Chaos

Diandian Diana Chen[1], Richard A. Gray[2], Ilija Uzelac[1], Conner Herndon[1], and Flavio H. Fenton[1]
[1]*School of Physics, Georgia Institute of Technology. and*
[2]*Food and Drug Administration*
(Dated: March 1, 2017)

It is widely believed that one major life-threatening transition to chaotic fibrillation occurs via spiral-wave breakup that is preceded by spatiotemporal dispersion of refractoriness due to alternations in the duration of the cardiac action potential (AP). However, recent clinical and experimental evidence suggests that other characteristics of the AP may contribute to, and perhaps drive, this dangerous dynamical instability. To identify the relative roles of AP characteristics, we performed experiments in rabbit hearts under conditions to minimize AP duration dynamics which unmasked pronounced AP amplitude alternans just before the onset of fibrillation. We used a simplified ionic cell model to derive a return map and a stability condition that elucidates a novel underlying mechanism for AP alternans and spiral breakup. We found that inactivation of the sodium current is key to developing amplitude alternans and is directly connected to conduction block and initiation of arrhythmias. Simulations in 2D where AP amplitude alternation led to turbulence confirm our hypothesis.

Many spatially extended oscillatory and excitable systems in biology, physics, and chemistry are known to exhibit spatiotemporal chaos[1–3], where complex-disordered signals in both time and space are often driven by defect-mediated turbulence of spiral-waves that continuously generate and annihilate in an irregular fashion, i.e. spiral-wave breakup[4]. Spiral-wave dynamics play a fundamental role in the study of cardiac dynamics[2] as they are often the underlying drivers of deadly arrhythmias such as tachycardia and fibrillation [2, 5–7].

Dynamically induced dispersion of refractoriness by a period-doubling bifurcation[8–10] in the duration of cardiac action potentials (APs) is considered to be the main substrate for spiral-wave breakup in the heart. The dispersion in AP repolarization resulting from cellular alternans in AP duration (Fig 1a) has been linked to alternans in the global electrocardiogram signal recorded from the body surface (Figure 3 supplement), and so-called T-wave alternans has been suggested as a biomarker for arrhythmia risk and survival rates [11]. Furthermore, a theoretical mechanism for this cellular bifurcation relates the slope of the AP duration (APD) restitution function (i.e., APD as a function of the preceding recovery time, also known as diastolic interval(DI)) to APD alternans[12, 13] at the cellular level and spiral breakup in tissue [14, 15]. However, other mechanisms such as memory, calcium dynamics[16–18], regional increases in K^+ levels[19], and conduction velocity restitution[9, 10, 18] have been shown to enhance or suppress this bifurcation independent of APD restitution slope.

While T-wave alternans can lead to regions with complex dispersion of refractoriness[20] recent experiments suggest that it is not necessarily cellular alternans in AP *duration* but rather in AP *shape*[21] and AP *amplitude*[22] that is significant in generating conduction block and spiral breakup. Furthermore, there is evidence of amplitude alternans in the QRS segment (corresponding to AP depolarization) of the electrocardiogram preceding the initiation of supraventricular tachycardia and during narrow QRS tachycardia[23]. These alternations have been shown to be rate-dependent, occurring only after an abrupt increase of rate above a critical value, and to be independent of the tachycardia mechanism[23]. This suggests a mechanism driven by cellular action potential amplitude (APA) alternans that is different to the one produced locally at small regions in between propagation and conduction block[20, 24, 25] (see Fig. 5 supplement) due to electrotonic currents. Understanding the mechanism of rate-dependent QRS alternans could lead to important clinical implications. To our knowledge, there are no previous detailed studies linking cellular mechanisms of APA to tissue-level alternans of the QRS complex in the electrogram.

In this manuscript we 1) demonstrate APA alternans in paced rabbit ventricles (Fig. 1b) using low-calcium Tyrode solution to minimize APD alternans which can mask other AP shape changes; 2) demonstrate that APA alternans are *not* due to conduction block (Fig. 3-5, supplement); 3) propose simple mathematical ionic cell models that reproduce experimentally measured voltage dynamics (Fig. 1, supplement); 4) derive a return map and corresponding analytical criterion for APA alternans (analogous to that for APD alternans[12, 13]); 5) demonstrate that APA alternans can generate QRS amplitude alternans in a 1D cable when paced at fast rates; and 6) demonstrate that these APA alternans can lead to conduction block and produce spiral breakup with spatiotemporal patterns reminiscent of cardiac fibrillation. Our results implicate rapid inactivation of the rapid sodium current as a possible target for preventing APA-alternans and the initiation of fibrillation.

Methods. All experimental procedures were approved by the office of Research Integrity Assurance of Georgia Tech under IACUC #A15034, see supplement for full details. Briefly, rabbit hearts (n=5) were optically mapped and Voltage signals where

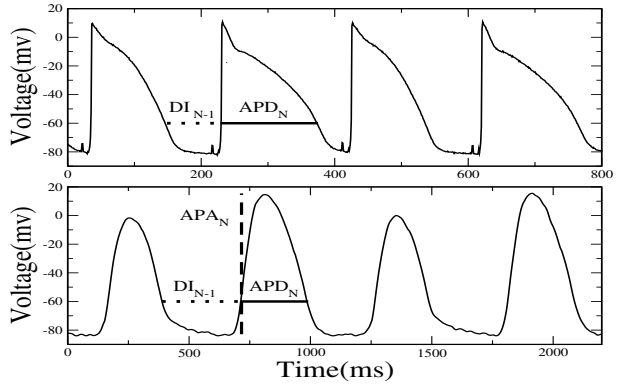

FIG. 1. Action Potential Alternans. A) endocardial microelectrode voltage signals from canine ventricles showing large alternans in APD (32 ms) but no alternans in APA. b) optical-mapping voltage signals from a pixel recorded from a rabbit ventricle surface perfused with low-calcium Tyrode's solution, low-flow to simulate ischemia and paced at a period of 550 ms. Horizontal dotted lines show measurement of DI, solid lines show measurement of APD, and the vertical dashed line APA.

recorded with normal and very-low calcium Tyrode (62.5 μMol Vs 2 mMol in normal) at pacing cycle lengths decreasing from 800ms until fibrillation. In all cases APA alternans appeared before the onset of fibrillation. For normal Tyrode, stable APD alternans (see supplement for definition) was present for many cycle lengths with APA alternans appeared just before fibrillation. For low-Ca Tyrode no APD alternans was observed and only APA alternans developed before fibrillation, see supplement for more details.

The APD map. The APD restitution map is a fundamental tool in the analysis of cardiac dynamics as it relates each APD to its previous diastolic interval[12, 13].

$$APD_{n+1} = R\left(DI_n\right) \tag{1}$$

$$APD_n + DI_n = T \text{ (constant)}. \tag{2}$$

Similarly, we assume that APA is a function of the previous diastolic interval (as shown in Fig. 1a). However, we further consider that the diastolic interval may be mapped to a state variable, the sodium inactivation recovery or h-gate[26] (shown as dashed line on Fig. 1b of the supplement). Therefore it's possible to find functions F and L such that

$$DI_n = L(h_n) \tag{3}$$

$$APA_{n+1} = F(h_n), \tag{4}$$

where h_n is the value of the sodium inactivation gate at the end of beat n. We also consider that APD is a function of the voltage's amplitude, $APD_n = G\left(APA_n\right)$, since the higher the maximum voltage amplitude the longer the APD could be. Therefore one can derive the relationship

$$T = G(APA_n) + L(h_n). \tag{5}$$

These relationships are the building blocks of our APA map. From this foundation we derive below a stability condition for the fixed point of the system as a function of the sodium inactivation gate variable h and period, T.

The APA map. Eqn. 4 we designate to be our APA restitution function. Then Eqn. 5 can be rearranged in the form

$$APA_n = G^{-1}(T - L(h_n)) = Y(h_n, T), \tag{6}$$

which we designate as our APA period function. Note that both functions G and Y are considered to be decreasing monotonically.

Together, the APA period function, $Y(h_n, T)$, and the APA restitution function, $F(h_n)$, can be used to analyze the stability of the period-one response as a function of period T through linearization. To enhance understanding, we condensed the two functions into one return map by taking Eqn. 6 and combining with Eqn. 4 by replacing the APA term in Eqn. 4.

$$Y(h_{n+1}, T) = F(h_n). \tag{7}$$

We can rearrange this function to a return map form

$$h_{n+1} = Y^{-1}(F(h_n), T). \tag{8}$$

Next, we linearize around h*, where h* is the fixed point, by having $h_n = h^* + \delta h_n$, then the stability condition for period-one cycling is given by

$$\left.\frac{\delta h_{n+1}}{\delta h_n}\right|_{h^*} = \left(\frac{\delta Y^{-1}(F(h_n), T)}{\delta F(h_n)}\right)\left(\frac{\delta F(h_n)}{\delta h_n}\right)\Bigg|_{h^*} = \frac{\left.\frac{\delta F}{\delta h_n}\right|_{h^*}}{\left.\frac{\delta Y}{\delta h_n}\right|_{h^*}} \tag{9}$$

Thus, the stability condition becomes

$$1 \leq \left|\frac{\text{slope of APA restitution function}}{\text{slope of period function}}\right|\Bigg|_{h^*} \equiv |\rho|\,. \tag{10}$$

In other words, the ratio ρ of the slopes of the two functions determines the stability of the system's fixed point. If the condition in Eqn. 10 is met, APA alternans may occur.

Simulations. To investigate the applicability of the stability condition given by Eqn. 10, we constructed a simplified ionic cell model of the form

$$\begin{aligned} \partial V/\partial t &= D\ \partial^2 V/\partial x^2 - I_{ion} \\ dh/dt &= (h_\infty - h)/\tau'_h, \end{aligned} \tag{11}$$

where V is the membrane voltage and h is the sodium inactivation gate. Since in the experiments very low-calcium concentrations were used, we can assume to a first approximation that the calcium current is small enough to be neglected from the modeling. Therefore we have the I_{ion} in Eqn. 11 consists of only two currents:

one for sodium and one for potassium ($I_{ion} = I_{Na} + I_K$). The equations and values for I_{Na} and I_K for the model are given in the supplementary material.

Integration of Eqn. 11 in single cells and in 1D leads to action potentials that match those obtained experimentally in the rabbit ventricles and Fig. 1 of the supplement. Furthermore, the model can produce AP alternans. To validate the predictions of Eqn. 10 we first numerically found the period for which alternans appears in the model by pacing the model in a single cell. The details of this protocol is in the supplement. This was achieved at a period of around $T_C = 371$ms with a critical h-gate value of $h_C = 0.450$. Next, while pacing the model faster, we measured the steady-state values of APD, DI, h-gate value, and APA as functions of T. From these values, we can extrapolate the restitution equation and the period equation (Eqs. 4 and 6, respectively). Fig. 2a shows the APA restitution function (solid line) for the model along with several period functions (dashed lines) calculated for different stimulation periods. The crossing of the period function and the restitution function is the fixed point of the system for that period. It can be noticed that while for this model the APA restitution has a relatively smooth slope, the slope of the period functions, at the fixed points, increases in magnitude as the period increases. Therefore according to Eqn. 10 larger periods are more stable as their ρ value will have magnitudes $<< 1$ agreeing with the numerical simulations. In fact according to the map relation, the critical period at which the slope of the two curves combine to one, $T_C = 370.8$ms and $h_C = 0.449$, closely matches the critical period obtained through pacing the numerical model. The maps in Fig. 2b show a cobweb diagram for two periods, one at 450ms and another at 367 ms. The first period line shows a stable fixed point and the second shows alternans since the period is below the critical period.

The functionality and predictability of the single variable return map (Eqn. 10) can further be extended to an analytic stability condition by considering some approximations to the F, G and L functions, giving then a better understanding of APA alternans development as a function of physiological parameters.

The following derivations are based on approximations of model behavior. Though cardiac dynamics is complex, we aim to gain intuitive understanding as a function of basic parameters and measurements, therefore it would be desirable to have a criteria in terms of physiological parameters.

For example, the h-gate for most cardiac cell models [27] follows an equation of the form given by Eqn. 11 which leads to a recovery of inactivation that could be approximated by an exponential

$$h_n = 1 - ae^{-DI_n/\tau_h}. \tag{12}$$

Furthermore, if we consider that the APD is proportional to the APA, that is

$$APD_n = \alpha APA_n + C_1, \tag{13}$$

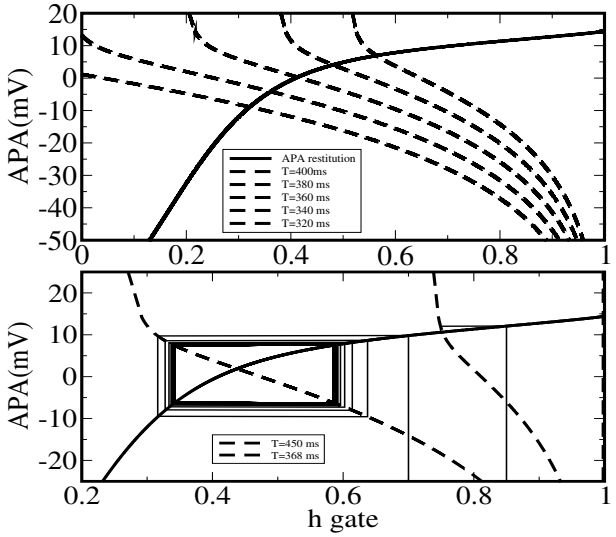

FIG. 2. Maps obtained for the numerical cell model. Top: amplitude restitution curve as a function of the recovery of the h-gate (solid) and period curves (dash) also as a function of h-gate for five different periods (320,340,360,380, and 400 ms). Bottom: cobweb diagram for a period with a stable fix point (450ms dashed) and for a period with alternans ($368ms$ solid). Notice that the values for the h-gate are bounded between 0 (closed) and 1 (fully open) and the APA alternates between -8 and 8 mV.

then a constant stimulation period can be given by

$$\begin{aligned} T &= APD_n + DI_n \\ &= \alpha APA_n + C_1 - \tau_h \left[\ln\left(1 - h_n\right) - \ln\left(a\right)\right]. \end{aligned} \tag{14}$$

If we further consider that to first approximation the APA is linear with respect to the recovery variable h, then

$$APA_{n+1} = \beta h_n + B_1. \tag{15}$$

Then the 1D map stability condition given by Eqn. 10 may be written as

$$\rho = \beta\alpha(h^* - 1)/\tau_h. \tag{16}$$

Note that we have dropped the absolute value bracket around ρ as the value of ρ is generally negative. This equation gives the guidelines for parameter values that can lead to APA alternans given simple numerical models. For example the parameters β, α, and τ_h are directly linked to the parameters g_{na}, I_k, and $\tau_{h'}$, respectively, in the model. Note that h^* depends on T, β, τ_h, and α through Eqns. 12, 13, 14, and 15. To validate the predictions of Eqn. 16 a fit was made to Eqns. 12, 13, and 15 using the model. This results in $\alpha = 262.7$, $\beta = 0.5371$ and $\tau_h = 80$. Using these values in the analytic Eqn. 16 it is possible to obtain ρ as a function of period and/or h^*. Here, our critical h_C value is 0.433 and critical T_C value is 366.25ms when ρ is equal to -1. This critical value matches closely the h_C obtained by the map functions (0.449 for h_C and 370.8ms for T_C) and by pacing

the numerical simulations of the cell model (0.450 for h_C, and 371ms for T_C) shown before. To further validate the predictions of Eqn. 16 we varied parameters in the model to modify the periods at which the model can generate APA alternans. As τ_h is multiplied with a factor from 0.5 to 2 the critical T_C changes from 355.5ms to 439.5ms as shown in figure 2 of the supplement. Furthermore, when τ_h is very large, the system no longer can produce APA alternans.

Numerical simulations of the model in a cable paced at fast rates showed that when APA alternans appeared, the calculated electrocardiogram results in QRS alternans, as shown in Fig. 3, similar to those observed in experiments and in the clinic[28, 29]. More importantly, simulations in 2D demonstrated that while APD alternans can be very large, no conduction block was present, however as APA developed then conduction block was possible as very small amplitudes will fail to propagate and will initiate spiral waves. This is consistent with our rabbit experiments, Fig. 4 top shows the voltage trace from an optical-mapping signal in a rabbit ventricle during fast pacing with very large APD alternans, and while dispersion is large, the dynamics is stable during the whole episode of several minutes of pacing. In contrast, Fig. 4 middle, shows that once large alternans in amplitude appeared fibrillation could appear, just as in our 2D numerical simulations as shown in Fig. 4 bottom.

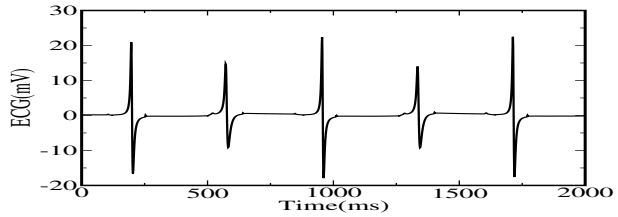

FIG. 3. Pseudo-ECG showing pronounced QRS (sharp peaks) alternans from a 1D cable of length 200 cells using the model after pacing four times as in Fig. 1 of the supplement. Note that since there is little change in APD, T-wave alternans is not very pronounced.[30].

Discussion. Alternans as a mechanism for arrhythmias has historically been dominated by studies focused on contraction alternans[31] and T-wave alternans [8–10, 20]. A few recent studies have shown that QRS alternans may be yet another mechanism for arrhythmia, particularly during narrow QRS tachycardias[23][32] where alternans has been shown to be a rate-related phenomenon that depends on an abrupt increase in rate activation above a critical frequency. Here, we derived a map and an analytic condition for when APA alternans can be expected at a cellular level and verified it with a numerical model. The numerical model showed that when paced in tissue at fast cycle lengths, it produces APA alternans in a single cell and resulted in conduction block in space. Recently Myles, *et al.* [22] have shown that cellular alternans of action potential amplitude is notably present in rabbit hearts with heart

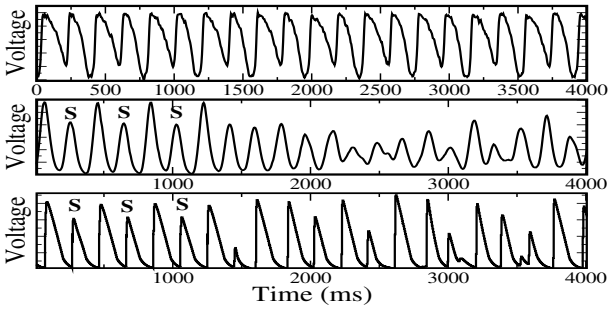

FIG. 4. Top: optical mapping voltage signal from one pixel from a rabbit heart with normal Tyrode paced at a fast period showing large APD alternans that's **stable**. Middle, similarly, signal from one pixel from rabbit ventricle with low-calcium Tyrode and during APA alternans just before initiation of fibrillation. Bottom, numerical model's voltage signal, in 2D, showing APA alternans before conduction block and initiation of arrhythmia.

failure and that APA is of particular importance in the initiation of VF, and in fact more important than APD alternans[22, 33]. They showed that post-infarction hearts are more vulnerable to ventricular arrhythmias at rapid rates and that APA alternans were associated with conduction block and VF. Similarly, clinical data [21] have indicated that APA is more important in the development of arrhythmias in heart-failure patients, and APA was suggested to be the mechanism for T-wave alternans rather than APD. Furthermore, several experimental studies have shown that it is possible to sustain large gradients of APD alternans[5, 8], even with several discordant alternans regions[20, 34] that are stable (*i.e.* nodal lines do not move) and without conduction blocks, and still have no APA alternans. However as the period is further decreased then the development of APA discordant alternans has been shown to appear[9, 22]. This can be linked to when the CV restitution starts to decrease in value[9] as there is a well known correlation between CV and APA[35]. Our experimental and numerical simulations agree with these previous results and show that it is possible to sustain large alternans in APD without the development of conduction block. This is because as long as the short APD can still preserve large amplitudes, it will be able to propagate. However once APA develops, a very short APA will be unable to propagate.

In this manuscript we linked cellular APA alternans to QRS alternans in the ECG and created a framework to characterize when a given model will display APA alternans. A major conclusion of our analysis is the importance of sodium current in the dynamics of APA alternans. We have used a simple 1D map, analogous to the APD restitution map but for APA, that leads to an APA alternans condition given by Eqn. 10. Cobweb diagrams of these maps show that indeed APA alternans will develop when parameters of the maps satisfy the cri-

teria. We have also introduced a simple cell model that can produce alternans in APA and showed that a map reconstructed from the model agrees with the condition. Furthermore, by using simplified functions to describe the dynamics of the system we have derived a simple analytic expression given by Eq.10 that predicts alternans as a function of physiological model parameters, as shown in Eqn. 16.

The simulations of the model equation in 1 and 2D show that APA alternans can lead to conduction block resulting in initiation of spiral waves and complex dynamics as observed experimentally. Our main result is that amplitude alternans-induced conduction block leading to spiral breakup can occur via inactivation of the sodium channel (that is, how quickly sodium channels fully recover). The analysis of the conditions for alternans indicate that sodium excitability, potassium, and the h-gate recovery are key to development, while calcium may be more important in the development of APD alternans. Our results suggest that targeting sodium-current inactivation dynamics (in addition to repolarization kinetics that generate APD alternans) should be considered as possible anti-arrhythmic strategies.

Acknowledgments. Work possible by NSF grants: CNS-1347015 and CNS-1446675.

[1] A. Goryachev and R. Kapral. *Phys. Rev. Lett.*, 76:1619–1622, Mar 1996.

[2] G. Bub *et al. Phys. Rev. Lett.*, 88:058101, Jan 2002.

[3] S.W. Morris *et al. Phys. Rev. Lett.*, 71:2026–2029, Sep 1993.

[4] M.C. Cross and P.C. Hohenberg. *Science*, 263:1569–1570, 1994.

[5] E.M. Cherry and F.H. Fenton. *New Journal of Physics*, 10(12):125016, 2008.

[6] R. A. Gray *et al. Circulation*, 91(9):2454–2469, 1995.

[7] R. A. Gray *et al. Nature*, 392(6671):75–78, 1998.

[8] J.M. Pastore *et al. Circulation*, 99(10):1385–1394, 1999.

[9] M.A. Watanabe *et al. J. Cardiovasc Electrophysiol*, 12 (2):196–206, 2001.

[10] Z. Qu *et al. Circulation*, 102(14):1664–1670, 2000.

[11] D. S. Rosenbaum *et al. New England Journal of Medicine*, 330(4):235–241, 1994.

[12] JB Nolasco and R.W. Dahlen. *J Appl Physiol*, 25(2): 191–196, 1968.

[13] M.R. Guevara *et al. Computers in Cardiology*, pages 167–170, 1984.

[14] M. Courtemanche. *Chaos*, 6(4):579–600, 1996.

[15] F. H. Fenton*et al. Chaos*, 12(3):852–892, 2002.

[16] E.G. Tolkacheva *et al. Physical Review E*, 67(3):031904, 2003.

[17] M.E. Díaz *et al. Circulation research*, 94(5):650–656, 2004.

[18] E.M. Cherry and F.H. Fenton. *American Journal of Physiology-Heart and Circulatory Physiology*, 286(6): H2332–H2341, 2004.

[19] Veniamin Y. Sidorov *et al. American Journal of Physiology-Heart and Circulatory Physiology*, 301(1): H209–H220, 2011.

[20] A. Gizzi *et al. Frontiers in physiology*, 4, 2013.

[21] S.M. Narayan *et al. Journal of the American College of Cardiology*, 52(22):1782–1792, 2008.

[22] R.C. Myles *et al. Journal of molecular and cellular cardiology*, 50(3):510–521, 2011.

[23] F. Morady *et al. Journal of the American College of Cardiology*, 9(3):489–499, 1987.

[24] H. Arce *et al. Chaos*, 10(2):411–426, 2000.

[25] F. H. *et al.* Fenton. *Journal of Veterinary Cardiology*, 10 (2):87–103, 2008.

[26] A.L. Hodgkin and A.F. Huxley. *The Journal of physiology*, 117(4):500–544, 1952.

[27] F.H. Fenton and E.M. Cherry. *Scholarpedia*, 3(8):1868, 2008.

[28] I. Uzelac *et al.* In *Engineering in Medicine and Biology Society (EMBC), 2016 IEEE 38th*, pages 3941–3944. IEEE, 2016.

[29] K. Gima and Y. Rudy. *Circulation Research*, 90(8):889–896, 2002.

[30] A.Bueno-Orovio *et al. Journal of theoretical biology*, 253 (3):544–560, 2008.

[31] B. Surawicz and C. Fisch. *Journal of the American College of Cardiology*, 20(2):483–499, 1992.

[32] Y.T. Tai *et al. Clinical Cardiology*, 14(12):1003–1006, 1991.

[33] Irma Marti*s*ienė *et al. BioMed research international*, 2015, 2015.

[34] Sergey Mironov *et al. Circulation*, 118(1):17–25, 2008.

[35] Robin M Shaw and Y. Rudy. *Circulation Research*, 80 (1):124–138, 1997.

[36] B. Echebarria and A. Karma. *Physical Review Letters*, 88(20):208101, 2002.

[37] F.H. Fenton *et al. Journal of Veterinary Cardiology*, 10 (2):87–103, 2008.

[38] W. H. Gaskell. *Philosophical Transactions of the Royal Society of London*, 173:993–1033, 1882.